THE BELL SYSTEM TECHNICAL JOURNAL
Vol. 57, No. 9, November 1978
Printed in U.S.A.

Caustic Patterns Associated With Melt Zones in Solidified Glass Samples—Part II: Asymmetric Cases

By J. B. SEERY, T. D. DUDDERAR, and P. G. SIMPKINS

(Manuscript received March 17, 1978)

Two types of geometrical asymmetries have been analyzed numerically to determine their influence on the externally visible caustic patterns from a drawdown zone. The first of these asymmetries involved axial displacement of identical opposing profiles of the drawdown zone, while the second involved opposing profiles of differing slope positioned with their inflection points in axial alignment. The results of these studies are presented graphically as an aid to interpreting the asymmetries of actual caustic patterns generated by illuminating real drawdown zone samples in optical fiber drawing.

I. INTRODUCTION

In the present study, we demonstrate how deviations from rotational symmetry in the melt zone give rise to asymmetries in the resulting caustic pattern. In Ref. 1, rotationally symmetric profiles of melt zones were generated by averaging measurements of data taken from solidified melt zone samples. These data provided symmetrically idealized data sets for the study of the two principal types of caustics as functions of the rate of change in the cross section. Changes in the maximum rate of change in the cross section were simulated by scaling* the data sets, and the analysis was carried out using the algorithms developed earlier in Ref. 2. These algorithms describe families of 2- and 3-intercept caustics as shown in Fig. 1a, where the scale factor is unity. The incident angle, β, for an axial light ray at the inflection point, I, is 52.9 degrees on both sides of the cross section. However, in Ref. 2 it was shown that the samples were usually asymmetric, resulting in pronounced asymmetric caustic patterns, especially when the caustic rays emerged nearly tangent to the surface.

* That is, by scaling the axial and transverse data values differently with the scale factor, SF = (axial scale)/(transverse scale).

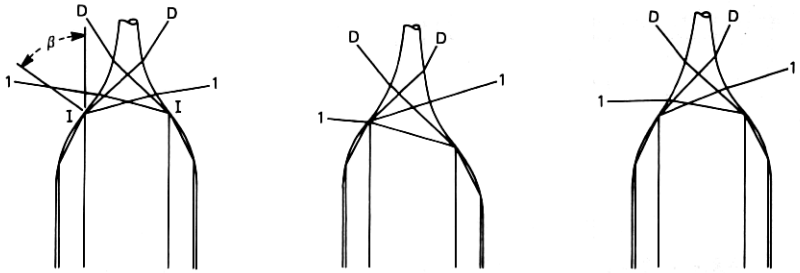

Fig. 1—Drawdown profiles for a melt zone with an average γ of 1.323 and a preform radius, R, of 0.1217 in. (3.09 mm). The data scale factor, *SF*, is 1. The rays labeled *D* represent the 3-intercept caustic trajectories and the rays labeled 1 represent the first 2-intercept caustic trajectories for the following cases: (a) Symmetric drawdown profiles with $\gamma = 1.323$ ($\beta = 52.9$ degrees) on both sides and no shift ($\Delta/\gamma R = 0.0$, $\delta\gamma = 0$ percent). (b) Asymmetric drawdown profiles with $\gamma = 1.323$ ($\beta = 52.9$ degrees) on both sides and an axial shift of $\Delta = 0.05$ in. (1.27 mm) of the left side ahead of the right side ($\Delta/\gamma R = 0.311$, $\Delta/R = \pm 0.41$). Here $\delta\gamma = 0$ percent. (c) Asymmetric drawdown profiles with $\gamma = 1.455$ ($\beta = 55.5$ degrees) on the left side and $\gamma = 1.1907$ ($\beta = 50.0$ degrees) on the right side (average $\gamma = 1.323$, $\delta\gamma = \pm 10$ percent). Here $\Delta/\gamma R = 0.0$.

Two types of asymmetric drawdown zones were studied, based upon the symmetric data set generated from the fourth sample.[1,2] In the simplest case, the asymmetry was introduced by axially shifting the profile data for one side of the cross section with respect to the other. An asymmetric cross section with the caustic rays is shown in Fig. 1b, where the relative axial shift between the two profiles is 41 percent of the preform radius* and the scale factor is 1.0. The asymmetry produces significant counterclockwise rotations in the propagation directions of the emerging caustic rays when viewed with the downstream profile as shown on the left.

A second type of asymmetry was produced by scaling the opposite sides differently. In this study, the inflection points of the opposite (differently scaled) profiles were kept in axial alignment so that the resulting shift in the caustic ray pattern would be due solely to the difference in the slopes, as shown in Fig. 1c. There the scale factors of opposite sides are 0.9 and 1.1. These produce counterclockwise rotations of the emerging caustic rays comparable to those shown in Fig. 1b and toward the elongated profile as plotted.

In addition, for both types of asymmetry, the overall scaling was changed so that the effects of these asymmetries could be assessed for greater or lesser average gradients than those of the original data. These scale factors and associated average slopes, γ, and incident angle values, β_A, are tabulated in Table I. Here γ is the average of the slopes of the two outer normals at the inflection points, dx/dy_I, and $\beta_A = -\text{arc tan } \gamma$.

The next two sections present the results from the computer simulations including diagrams of significant cases for both types of asymme-

* $R = 0.1217$ in. or 3.09 mm.

Table I—Scale factors and average slopes and angles

Scale Factor	Average Outer Normal Slope γ	Average Incidence Angle β_A (degrees)
1.300	1.720	59.8
1.200	1.588	57.8
1.000	1.323	52.9
0.775	1.025	45.7
0.700	0.926	42.8
0.520	0.688	34.5
0.450	0.595	30.8
0.340	0.450	24.2

tries. The reader who requires a less detailed synopsis of these results is referred to the discussion portions of these sections and to Section V, Summary.

II. SHIFT ASYMMETRY

The effects of axial misalignments in the profiles of the drawdown zone were studied by computing the ray paths for examples with the profiles of opposite sides shifted various amounts, Δ. The results of these computations provide a complete description of the caustic patterns for an asymmetric drawdown zone with a range of profile shifts for each γ given in Table I.

To compare the varied scalings, an asymmetry parameter, $\Delta/\gamma R$, was established, where R is the preform radius. The asymmetry was varied from $0 \leq |\Delta/\gamma R| \leq 1.20$, which represents a broader range than is ever likely to actually occur in fiber drawing. The specific incremental changes in asymmetry were chosen to illustrate what occurs as the asymmetry increases.

An extreme example of the effects of this type of asymmetry can be seen by comparing Fig. 2a with Fig. 2b, which has the same average slope but a large asymmetry. Emergent 2-intercept caustics are labeled numerically to indicate which of the family they represent; the 3-intercept caustics are labeled D. The unlabeled rays represent caustic rays of the 1-intercept family which emerge at the inflection point for γs less than 0.939. In Fig. 2b, the 3-intercept caustics have rotated counterclockwise, or in a positive direction, toward the leading side. Extra 2-intercept caustics (labeled 2′, 2″, 3′) have merged on the leading side, while all 2-intercept caustics have disappeared from the trailing side. Those 2-intercept caustics on the $+\Delta$ side have rotated clockwise, in a negative direction, away from the leading side.

2.1 Graphical results

Figures 3a to 3d are simplified versions of the format used in Figs. 1 and 2 which show both the internal ray paths and the external caustic trajectories. In these simplified diagrams, the internal ray paths have

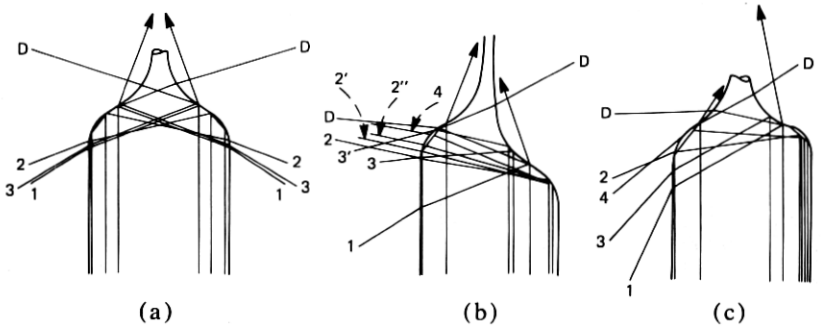

Fig. 2—Drawdown profiles for a melt zone with an average γ of 0.688 ($SF = 0.52$). The rays labeled D represent the 3-intercept caustic trajectories, while the rays labeled 1, 2, 3, etc., represent the first, second, third, etc., 2-intercept caustic trajectories for the following cases; (a) Symmetric drawdown profiles with $\gamma = 0.688$ ($\beta = 34.5$ degrees) on both sides and no shift, $\Delta/\gamma R = 0.0$, $\delta\gamma = 0$ percent. (b) Asymmetric drawdown profiles with $\gamma = 0.688$ ($\beta = 34.5$ degrees) on both sides and a shift, $\Delta = 0.075$ in. (1.905 mm) of the left side ahead of the right side ($\Delta/\gamma R = \pm 0.896$, $\Delta/R = \pm 0.616$). Here, $\delta\gamma = 0$ percent. (c) Asymmetric drawdown profiles with $\gamma = 0.894$ ($\beta = 41.8$ degrees) on the left side and $\gamma = 0.482$ ($\beta = 25.7$ degrees) on the right side ($\gamma = 0.688$, $\delta\gamma = \pm 30$ percent). Here, $\Delta/\gamma R = 0.0$.

been eliminated, and the drawdown profiles have been reduced to tangent lines at the inflection points. The profiles, shown as thick lines, meet in the symmetric case and progressively move farther apart to depict increasing $\pm\Delta$s. The external caustic trajectories are shown schematically as rays radiating from the point $\Delta = 0$. The 3-intercept caustics are again labeled D and, in the unusual case of a second 3-intercept caustic, $D2$ is used. Whenever the ray which internally reflects from the inflection point, I, is refracted from the opposite side without forming an external caustic, it is shown by an unlabeled dashed line. In Figs. 3a to 3d, the diagrams are drawn with the leading side as the left profile, consistent with Figs. 1b and 2b. We then define a positive, or forward, rotation of caustic angles to be counterclockwise, or toward the leading side.

We begin with gradually tapered profiles that emit little light. As the taper is increased, we observe an increase in the amount of light emitted and in the complexity of the caustic structure. The first case, with $\gamma = 1.72$, is shown in Fig. 3a. Both caustics present initially rotate in a forward direction as the asymmetry increases. However, the 3-intercept caustics quickly disappear from the trailing side by internal reflection. The 2-intercept caustics continue to rotate in a positive direction on the trailing side, but on the leading side they reverse direction and rotate in a negative direction at an asymmetry $\Delta/\gamma R$ of about 0.40. The situation is similar for $\gamma = 1.588$, not shown. The 3-intercept caustics also rotate forward. Since the emergent angle for the symmetric case is smaller this time (163.48 degrees as opposed to 172.66 degrees), the caustic does not internally reflect as soon. The 2-intercept caustic initially rotates forward. This time, the direction reversal on the leading side occurs earlier at a $\Delta/\gamma R$ of 0.33 and is more pronounced. Reducing γ to 1.323 does not

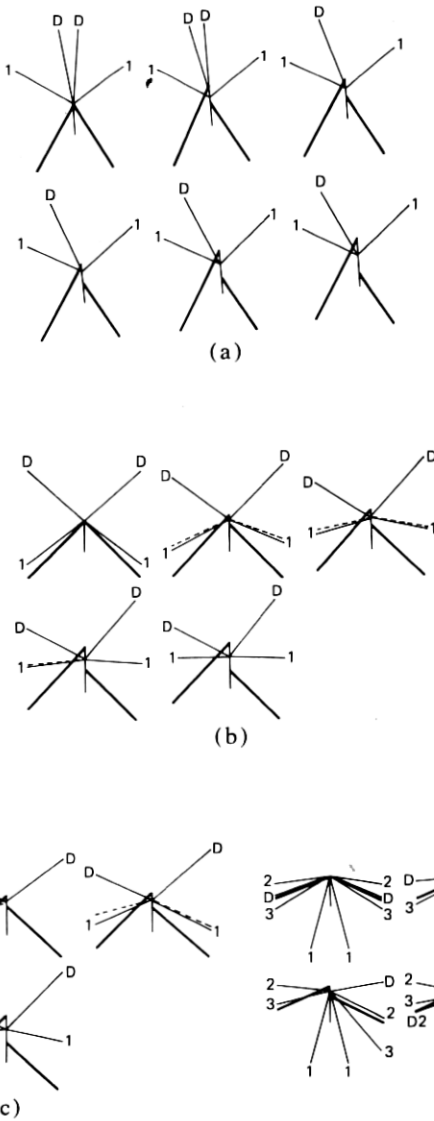

Fig. 3—Diagrams of external caustic trajectories for drawdowns of varying asymmetry due to axial shifts, $\Delta/\gamma R$, of varying amounts as follows: (a) For $\gamma = 1.720$ ($\beta = 59.8$ degrees), $\Delta/\gamma R = \pm 0.000, \pm 0.118, \pm 0.236, \pm 0.354, \pm 0.472, \pm 0.596$. (b) For $\gamma = 1.025$, ($\beta = 45.7$ degrees), $\Delta/\gamma R = \pm 0.000, \pm 0.199, \pm 0.410, \pm 0.596, \pm 0.801$. (c) For $\gamma = 0.926$ ($\beta = 42.8$ degrees); $\Delta/\gamma R = \pm 0.000, \pm 0.223, \pm 0.441, \pm 0.664, \pm 0.888$. (d) For $\gamma = 0.450$ ($\beta = 24.2$ degrees); $\Delta/\gamma R = \pm 0.000, \pm 0.183, \pm 0.365, \pm 0.548, \pm 0.730, \pm 0.913$. Here the sides of the melt zone are represented by heavy lines sloped β degrees below horizontal and shifted vertically in proportion to the axial shift, Δ. The external caustic trajectories are shown as rays emanating from a common center at their appropriate angles and labeled with D or $D2$ to indicate a first or second 3-intercept caustic and 1, 2, or 3, etc. to indicate a first, second or third, etc. 2-intercept caustic. Dashed lines represent emergent I rays which do not form caustics.

alter the situation significantly, except that both caustics are present for the entire range of asymmetry. In all cases, the rotation of all caustics on the trailing side has been consistently positive. On the leading side, the 2-intercept caustic's forward rotation reverses at a $\Delta/\gamma R$ of only 0.25. At the same time, a reversal in the forward rotation of the 3-intercept caustic also becomes apparent at an asymmetry of 0.75.

Figure 3b shows the case of $\gamma = 1.025$, where $\beta = 45.7$ degrees, i.e., very close to the 2-intercept caustic's extinction angle. This caustic emerges at a minimum angle, θ, for the symmetric case, and progressively forms larger angles as Δ increases; i.e., it rotates negatively on the leading side and positively on the trailing side. As discussed in Part I,[1] the rays which are only incident once on the first side form a catacaustic at the inflection point. If the catacaustic ray then refracts from the second side, it is *usually* seen as the first 2-intercept caustic ray. However, the dashed lines shown in the diagrams for the smaller asymmetries in Fig. 3b depict emergent rays which form internal catacaustics at the inflection points but are *not* seen as external caustics. We call these rays the *I* rays. Their angles are at least half a degree different from the 2-intercept caustic angles. Once the asymmetry has increased to a $\Delta/\gamma R$ of 0.80, however, these two rays have recombined. The 3-intercept caustic rotates in the forward direction over the asymmetry range studied.

Continuing further, the symmetric case with $\gamma = 0.926$ has no emergent 2-intercept caustic (see Fig. 3c). However, once the asymmetry has increased to $\Delta/\gamma R = 0.441$, the original 2-intercept caustic has re-emerged and subsequently rotates to larger θ angles on both sides. Again, the (noncaustic) *I* ray is initially distinct from the 2-intercept caustic ray, and they merge as the asymmetry increases. It should be noted that the *I* ray initially emerges on the forward side without forming a caustic before the 2-intercept caustic emerges. The 3-intercept caustic continues to rotate in a forward direction up to the largest calculated asymmetry, at which point it reverses direction on the forward side.

When γ is 0.688, there are three 2-intercept caustics for the symmetric case caused by multiple-folding in the fan of emerging light. This is the case shown earlier in Fig. 2a ($\Delta/\gamma R = 0.0$) and Fig. 2b ($\Delta/\gamma R = 0.896$). The folding geometry is illustrated in the left and center diagrams in Fig. 4a. Here the caustic rays are labeled 1, 2, 3, etc., consistent with the present convention, while the bounding rays are labeled L1, L2, L3, etc. The lower L numbers represent bounding rays originally propagating nearest the surface of the sample, with successive higher numbers proceeding inward. The left diagram in Fig. 4a shows that the fan of light which lies between bounding rays L3 and L4 is folded to form the three 2-intercept caustics with the first and third very nearly superimposed. As the asymmetry is increased, most of the 2-intercept caustics disappear on the trailing side while several additional ones appear on the leading

side. All these caustics rotate in a negative direction except for the original 2-intercept caustic on the leading side, which remains stationary. This unusual circumstance occurs because the I ray does not form an external caustic until its point of emergence has moved upstream of the melt zone to where the radius is constant.

In Fig. 2b, we can see that, since the profile on the initial incident side does not change, the internal trajectory of the I ray remains the same. Consequently, as long as caustic ray 1 refracts from the leading side its external angle will be constant, regardless of the magnitude of Δ. On the trailing side, the internal I ray is incident along that portion of the melt zone profile for which the radius is changing very rapidly; therefore, although it emerges for asymmetries of less than 0.3 it does not form an external caustic. However, this I ray reappears along with a first 2-intercept caustic when the asymmetry $\Delta/\gamma R$ reaches 1.2. In addition, a new 2-intercept caustic emerges on the leading side. This fourth 2-intercept caustic is associated with the closing of the break between the L1–L2 fan of light and the L3–L4 fan of light, illustrated in the center diagram in Fig. 4a. Consequently, this new caustic is folded downstream in the same way as the original first 2-intercept caustic. It originates from a coaxial ray initially propagating down the sample at a greater radius than the second 2-intercept caustic, but well inside the ray which originates the 3-intercept caustic, as shown in Fig. 2b.

Several other minor 2-intercept caustics appear and are labeled 2′, 2″, and 3′ in Fig. 4a center. These lie very close—in terms of both originating axial rays and emergent angles—to the second or third 2-intercept caustics. Each is associated with another fold in the fan of light.* The 3-intercept caustics in this case ($\gamma = 0.688$) initially rotate positively. Eventually, on the leading side this caustic reverses its rotation at $\Delta/\gamma R \simeq 0.6$ and then extinguishes at an asymmetry of about 0.8. On the trailing side, it continues to rotate in a forward direction. The additional 2-intercept caustics also appear in the case where $\gamma = 0.595$. Again the first 2-intercept caustic, when it emerges, remains stationary. The others in this family all rotate in the negative direction. The first, second, and third 2-intercept caustics emerge on the leading side for all asymmetries and are extinguished when the asymmetry is between 0.83 and 1.1 on the trailing side. Minor caustics associated with the second and third major caustics were found on the trailing side, but not on the leading side. The fourth caustic emerges at greater asymmetry than in the previous case of $\gamma = 0.688$ and again only on the leading side. This case, with $\gamma = 0.595$, is of particular interest because it exhibits for the first time a second 3-intercept caustic. The new caustic is associated with a folding

* It should be noted that, since the algorithm computes the ray trajectories for an equally spaced sequence of axial rays, finding these minor perturbations in emergent ray angles depends somewhat on the ray spacing chosen.

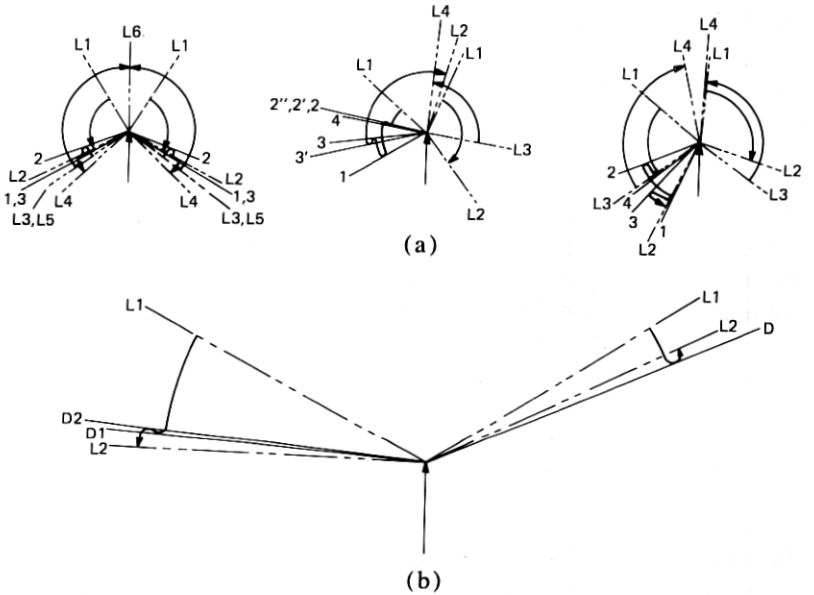

Fig. 4—(a) Schematic diagrams showing the external limiting rays for the 2-intercept light paths. The drawdown melt zone profiles are omitted, but the orientation is the same as in Figs. 1 and 2. The vertical arrow represents the incoming beam of collimated light illuminating the sample which in turn deflects the light into the plotted ray paths in the far field. Here, the solid lines represent the caustic trajectories and the broken lines represent the bounding rays limited by internal reflection (see Ref. 1). The circumferential arrows follow the continuous fan of light from the outermost bounding ray to the innermost bounding ray including all caustic rays. The bounding rays are numbered in sequence, beginning with L1 as the ray which originates nearest the surface of the sample and increasing inward L2, L3, etc. The caustic rays themselves are numbered 1, 2, 3, etc. to indicate that they represent the first, second, or third, etc. of the 2-intercept caustics. The asymmetries are as follows: *Right*—Symmetric, with $\gamma = 0.688$ ($\beta = 34.5$ degrees) on both sides and $\Delta/\gamma R = 0.0$, $\delta\gamma = 0$ percent. *Center*—Asymmetric with $\gamma = 0.688$ ($\beta = 34.5$ degrees) on both sides and a shift $\Delta = 0.075$ in. (1.905 mm) of the left side ahead of the right side ($\Delta/\gamma R = \pm 0.896$, $\Delta/R = \pm 0.616$). Here, $\delta\gamma = 0$ percent. *Left*—Asymmetric with $\gamma = 0.894$ ($\beta = 41.8$ degrees) on the left side and $\gamma = 0.482$ ($\beta = 25.7$ degrees) on the right side ($\gamma = 0.688$, $\delta\gamma = \pm 30$ percent). Here, $\Delta = 0.0$. (b) Schematic diagram showing external limiting rays for the 3-intercept light paths. The same ray identifications apply to the diagram as apply to the diagrams in Fig. 4a except that the caustics are numbered D and $D2$, representing the original and second 3-intercept caustics. The asymmetry is given by $\gamma = 0.595$ ($\beta = 30.8$ degrees) on both sides and a shift, $\Delta = 0.08$ in. (2.032 mm) of the left side ahead of the right side ($\Delta/\gamma R = \pm 1.105$, $\Delta/R = \pm 0.657$). Here, $\delta\gamma = 0$ percent.

in the fan of light in the direction opposite that of the original 3-intercept caustic. It is formed from a ray initially propagating down the fiber at a radius smaller than that ray which forms the first 3-intercept caustic. The folding pattern is shown in Fig. 4b, where the new ray is labeled $D2$. The new caustic emerges only for large asymmetry and only on the leading side. Meanwhile, the original 3-intercept caustic, as before, rotates initially in a positive direction but eventually reverses with increasing asymmetry.

The last case studied, $\gamma = 0.450$, is shown in Fig. 3d. Here the first three 2-intercept caustics emerge over the whole range of asymmetries.

The second and third caustics rotate in a negative direction; the first is again stationary. The fourth caustic emerges on the leading side and only for the largest asymmetry. The first 3-intercept caustic appears only on the trailing side and rotates downstream with increasing asymmetry. The second 3-intercept caustic appears alone on the leading side and only for larger asymmetries.

2.2 Discussion

The diagrams in Fig. 3 illustrate the far-field caustic response to increasing axial asymmetry $\Delta/\gamma R$ for fixed γ. We now present a general quantitative description of the caustic behavior due to changing geometry. Figure 5 shows the propagation angles, θ, of the major caustics as functions of $\Delta/\gamma R$ for various γ. The values, θ_-, for the trailing side are plotted to the left and the values, θ_+, for the leading side are plotted to the right of the zero asymmetry line. Figures 5a and 5b show the first 2-intercept and the 3-intercept caustics, respectively. The behavior of the remaining major 2-intercept caustics, the second, third, and fourth, are plotted in Fig. 5c. Each curve on these plots represents a fixed outer normal slope γ over the range of asymmetry tested. Those curves with arrowheads at the ends indicate caustics which emerge for higher asymmetry but were not calculated. The absence of an arrowhead indicates that the caustic ceases at or just beyond that point.

Other measures of caustic behavior are given in Fig. 6, for cases where the caustics emerge on both sides of the drawdown. In terms of actual three-dimensional drawdown samples, the caustic trajectories form cones of light whose total included angle is $\theta_- + \theta_+$. The average sum, $\theta_S = \frac{1}{2}(\theta_- + \theta_+)$, is plotted to show the half cone angle as a function of asymmetry. The average difference, $\theta_D = \frac{1}{2}(\theta_- - \theta_+)$, is plotted to show the rotation of the cone as a function of asymmetry. Figures 6a and 6c refer to various 2-intercept caustics, while Fig. 6b refers to the 3-intercept caustics.

Consider the first 2-intercept caustic shown in Figs. 5a and 6a. In Fig. 5a, starting with large γ, on the leading side θ^{U1} decreases, reaches a minimum, and slightly increases as $\Delta/\gamma R$ increases. As the profile becomes blunter, the minimum becomes more pronounced and moves toward the symmetric case, $\Delta/\gamma R \to 0$. When $\gamma = 0.926$, the drop in θ^{U1} as $\Delta/\gamma R \to 0$ becomes so large that the caustic is extinguished for small asymmetries and only the ends of the curve remain. This means that, although the first 2-intercept caustic is extinguished by internal reflection in the symmetric sample of $\gamma = 0.926$, the development of sufficient asymmetry causes an almost simultaneous reappearance on both sides of the sample. Figure 6a also shows that the average angle, θ_S^{U1}, of the first 2-intercept caustic decreases as $\Delta/\gamma R \to 0$. This decrease is greatest for profiles with the lowest γs. In other words, the caustic cone angle increases as the asymmetry increases, especially in blunt samples.

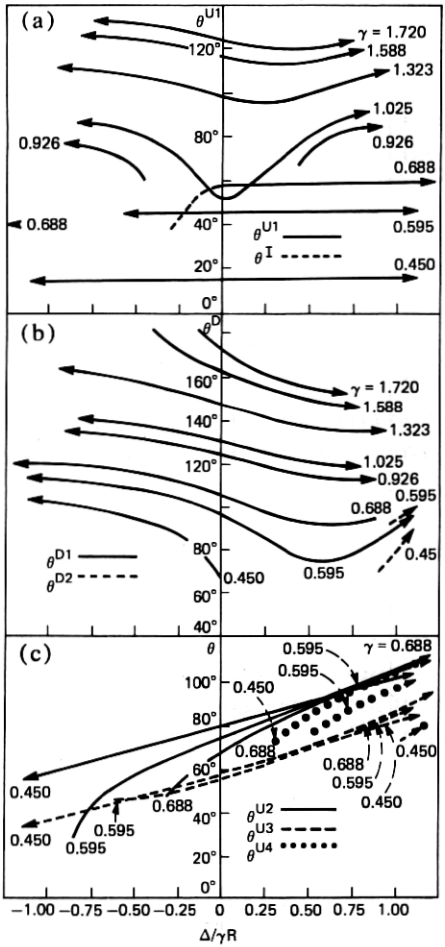

Fig. 5—Plots of the θ angles of the caustic trajectories for various γs as functions of the axial shift, Δ. Here the values of the angles, θ_+, of the caustics emergent on the leading side are plotted on the right and the values of the caustic angles, θ_-, of those emergent on the trailing side are plotted on the left. These results are arranged as follows: (a) The first 2-intercept caustic angles, designated θ^{U1}, and the I ray propagation angle, θ^{I}, vs $\Delta/\gamma R$. (b) The first and second 3-intercept caustic angles, θ^{D} and θ^{D2}, vs $\Delta/\gamma R$. (c) The second, third, and fourth 2-intercept caustic angles, θ^{U2}, θ^{U3} and θ^{U4}, vs $\Delta/\gamma R$.

At the same time, the θ_D^{U1} vs $\Delta/\gamma R$ curves in Fig. 6a show that the first 2-intercept caustic cone, which is initially symmetric about the drawing axis, first rotates toward the leading side, reverses, and then rotates back toward the axis as the asymmetry increases.

The 3-intercept caustic exhibits similar behavior, as shown in Figs. 5b and 6b, although there are significant differences. Again, there is a minimum in the caustic angle vs asymmetry curve that appears on the leading profile side of the θ^{D} vs $\Delta/\gamma R$ plot. However, the minimum does

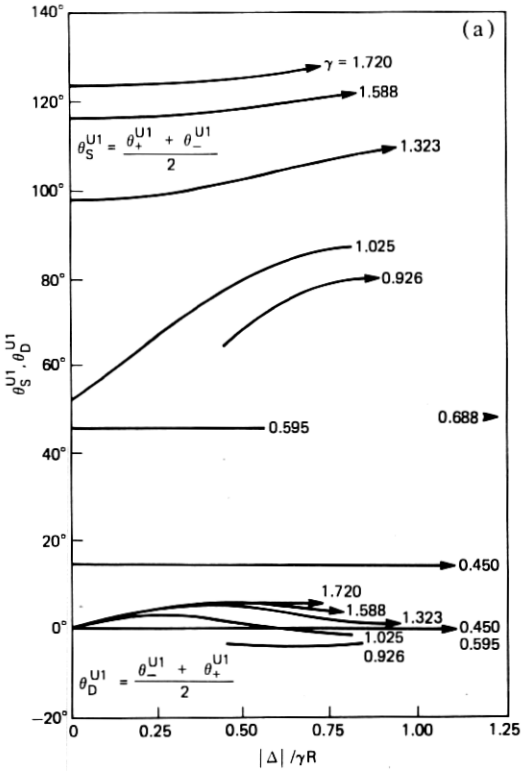

Fig. 6—Plots of the averaged sums, $\theta_S = \frac{1}{2}(\theta_- + \theta_+)$, and the averaged differences, $\theta_D = \frac{1}{2}(\theta_- - \theta_+)$, vs the magnitude of the axial shift $|\Delta|/\gamma R$ for various γs. These results are arranged as shown in 6a, 6b, and 6c. (a) The first 2-intercept caustic angles, θ^{U1}, averaged sums and differences vs $|\Delta|/\gamma R$. (*Figs. 6b and 6c on following pages.*)

not move toward the symmetry axis as γ decreases. Also, except in the region near the extinction points, the θ^D vs $\Delta/\gamma R$ plots are morphologically similar. In Fig. 5b, the magnitude of the depression in the curve still grows as γ decreases until, by $\gamma = 0.450$, the caustic is extinguished on the leading side. Figure 6b shows that the caustic cone half-angles, θ_S^D, are less influenced by the asymmetry than they were for the 2-intercept caustics (Fig. 6a). In addition, the 3-intercept caustic cone rotates more rapidly toward the leading side before it reverses direction, as shown by the θ_D^D curves in Fig. 6b. The behavior of the second, third, and fourth 2-intercept caustics is illustrated in Figs. 5c and 6c. These caustics are distinct because their directions of rotation are opposite those of the first two major caustics. This backward rotation, with increasing $\Delta/\gamma R$, of the second and third 2-intercept caustics parallels the reverse θ_A rotation with increasing γ noted in the earlier "symmetric" study.[1] At the same time, the θ_S values in the second and third 2-intercept caustics remain almost constant, indicating that the shapes of these caustic cones are

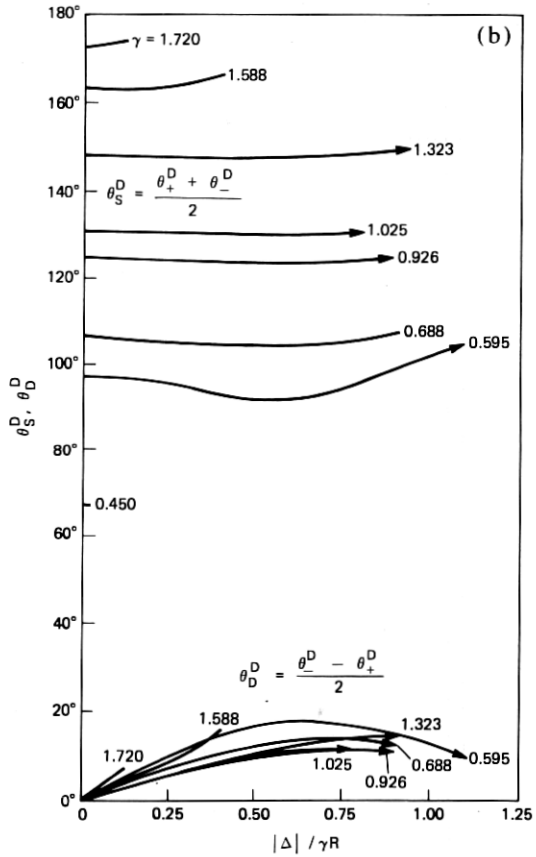

Fig. 6(b)—The 3-intercept caustic angles, θ^D, averaged sums and differences vs $|\Delta|/\gamma R$.

almost independent of the asymmetry, except near the extinction points.

III. DIFFERENTIAL SLOPE ASYMMETRY

The effects of asymmetric profiles of differing slopes were studied by changing the scaling of opposite sides of the profile by equal positive and negative percentages. These changes produce equal percentage changes in the slopes of the outer normals to the profiles, dx/dy. As shown in Part I,[1] the outer normal slope defines a unique incidence angle and is the most significant single parameter controlling the formation of the caustics. Therefore, we can define asymmetry by a ± change in γ, i.e., $\delta\gamma$.

An extreme example of the effects of this type of asymmetry is found in the comparison between Figs. 2a and 2c where in the latter $\delta\gamma = \pm 30$ percent. It can be seen that the external trajectories of the 3-intercept

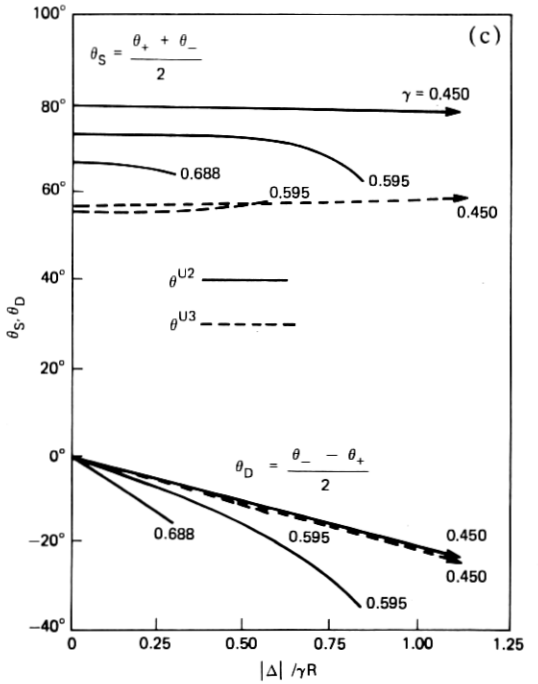

Fig. 6(c)—The second and third 2-intercept caustic angles, θ^{U2} and θ^{U3}, averaged sums and differences vs $|\Delta|/\gamma R$.

caustics have rotated in the direction of increasing γ, i.e., downstream on the shortened side and upstream on the lengthened side, which will be referred to as a forward (positive) rotation. At the same time, the external 2-intercept caustics have disappeared from the side of diminished γ, while an additional 2-intercept caustic, the fourth, appears on the opposite side. Like the 3-intercept caustic rays, the first and third 2-intercept caustic rays have rotated forward, while the direction of the second ray is unchanged. Indeed, only the insignificant 1-intercept caustics exhibit a backward or negative rotation. A better understanding of this behavior can be obtained only in the context of a range of changing asymmetries for the various average γs in Table I, which are discussed below.

3.1 Graphical results

A graphical description of the effects of this asymmetry covering a range of typical average γs is presented in Fig. 7. As in Fig. 3, these diagrams are simplified versions of the earlier formats showing only the external caustic trajectories. In most cases, the range of asymmetry, $\delta\gamma$, is from ± 0 to ± 30 percent. These represent a much greater range of asymmetry than might be expected to arise with actual samples. The

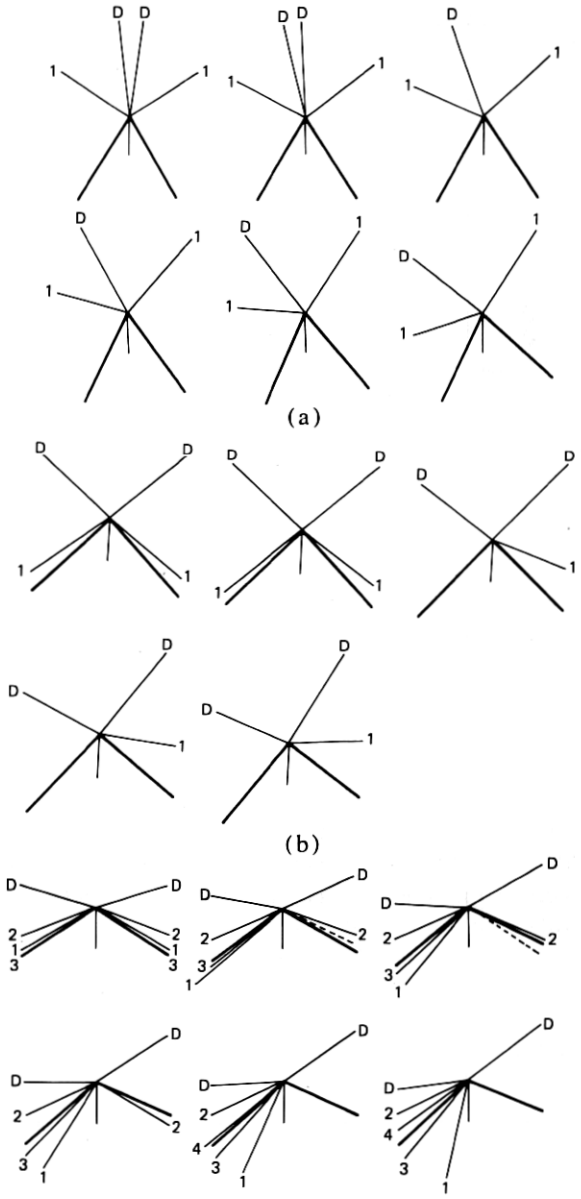

Fig. 7—Diagrams of external caustic trajectories for drawdowns of varying asymmetry due to percentage differences in γ, $\delta\gamma$, of varying amounts as follows: (a) $\gamma = 1.720 \pm 0\%$, $\pm$ 5%, $\pm$ 10%, $\pm$ 20%, $\pm$ 30%, $\pm$ 40%. (b) $\gamma = 1.025 \pm 0\%$, $\pm$ 1%, $\pm$ 10%, $\pm$20%, $\pm$ 30%. (c) $\gamma = 0.688 \pm 0\%$, $\pm$ 10%, $\pm$ 20%, $\pm$ 25%, $\pm$ 30%, $\pm$ 35%. Here the sides of the melt zone are represented by heavy lines sloped β degrees below horizontal. The external caustic trajectories are shown as rays emanating from a common center at their appropriate angles and labeled D to indicate a 3-intercept caustic and 1, 2, or 3, etc. to indicate a first, second, or third, etc. 2-intercept caustic. Dashed lines represent emergent I rays which do not form caustics.

specific incremental changes in asymmetry shown are not uniform, but were chosen to illustrate what occurs as the asymmetry increases. In every case, the diagram is drawn with the side of reduced γ to the left so that a forward (positive) rotation of caustic rays is consistently counterclockwise on the diagram. In general, on the *decreasing* γ side, θ *increases* and on the *increasing* γ side, θ *decreases* with increasing asymmetry.

The first two cases, for which $\gamma = 1.720$ (Fig. 7a) and 1.588, are similar; the rotation of all the caustic rays is forward and the 2-intercept caustic on the right-hand, or decreasing γ, side disappears by internal reflection. It initially propagates at a greater angle for $\gamma = 1.720$ than it does for $\gamma = 1.588$, and its rotation due to increasing asymmetry is positive. Therefore, the right-hand 2-intercept caustic extinguishes at a $\delta\gamma$ of only ± 10 percent for the case of $\gamma = 1.720$, but must reach a $\delta\gamma$ of ± 14 percent before it extinguishes for $\gamma = 1.588$. Decreasing γ to 1.323 reduces θ for all trajectories and permits forward rotations of both caustic rays on both sides for asymmetries up to $\delta\gamma = \pm 30$ percent without loss by internal reflection.

Internal reflection can also cause a caustic ray to disappear when its propagation direction swings too far upstream (θ decreasing). This is shown in Fig. 7b where the 2-intercept caustic ray on the increased γ side disappears as soon as the asymmetry begins to develop, because it emerges near the extinction region.[1] Very little asymmetry is then required to rotate the left-hand ray below the critical angle.

The case of $\gamma = 0.926$ lies within the range for which no 2-intercept caustic rays emerge from a symmetric drawdown. However, an asymmetry of ± 24 percent yields an external 2-intercept caustic ray on the side of reduced γ. Hereafter, the ray rotates in the forward direction, as do the 3-intercept rays. It is interesting to note that the I ray initially emerges on the reduced γ side at ± 22 percent asymmetry without forming an external caustic and becomes the externally visible caustic ray at $\delta\gamma = \pm 24$ percent. A similar ray, initially incident at the inflection point on the reduced γ side as a catacaustic ray, emerges even earlier on the increased γ side, at an asymmetry of $\delta\gamma = \pm 20$ percent. However, within the range of asymmetries considered, this ray never develops into an external caustic.

Reducing the γ to 0.688 creates a far more complicated structure even for the symmetric case, for which there are three 2-intercept caustics associated with multiple folds in the fan of emerging light. As shown earlier in Figs. 2a and 2c and further in Fig. 7c, the rotation is in general forward, although the second 2-intercept caustic appears to be relatively less responsive. On the decreased γ side, the fold in the fan of emerging light disappears by $\delta\gamma = \pm 10$ percent, leaving the I ray still emergent. No first or third 2-intercept caustics are formed. At $\delta\gamma = \pm 25$ percent, even the I ray has disappeared. At $\delta\gamma = \pm 30$ percent, the second

2-intercept caustic is extinguished on the reduced γ side and a fourth 2-intercept appears on the opposite side. A better understanding of this new caustic, which is the only one that rotates backward as shown by the last two diagrams of Fig. 7c, may be obtained from consideration of the left and right diagrams of Fig. 4a. As mentioned above, the left diagram in Fig. 4a shows that the fan of light which lies between bounding rays L3 and L4 is folded to form the three 2-intercept caustics with the first and third very nearly superimposed. The right side of Fig. 4a shows the same situation on the increased γ side for the asymmetric case represented by Fig. 2c with the folds of the first and third 2-intercept caustics widely separated. The break in the 2-intercept fan of light shown lying between bounding rays L2 and L3 in the left diagram in Fig. 4a (which separates the initial fan L1–L2 from the folded fan L3–L4) is closed in the right diagram by the new or fourth 2-intercept caustic. This new caustic is folded downstream in the same way as the original first 2-intercept caustic and originates from a coaxial ray initially propagating axially down the sample at an even greater radius than the second 2-intercept caustic but well inside the ray which originates the 3-intercept caustic (see Fig. 2c).

At a further reduction of scale to a γ of 0.595, all rays rotate forward due to increasing asymmetry, with the first 2-intercept the fastest and the second 2-intercept the slowest. In this case, the former disappears for the increased γ side at an asymmetry of almost ± 30 percent, while the fold in the fan of light separating the first and third 2-intercept caustic rays on the opposite side is almost completely suppressed by an asymmetry of only ± 20 percent.

A final case, at a γ of 0.450, behaves in much the same way, although since the θ angles are even smaller, the first 2-intercept caustic disappears from the increased γ side of the drawdown zone at an asymmetry of only ± 4 percent. In this case the 3-intercept caustic propagates at a lesser angle than the first 2-intercept caustic and disappears at around the same percent asymmetry and on the same side.

3.2 Discussion

Study of the collective response yields two general observations. First, it is apparent that all of the significant caustic rays rotate in a forward direction with increasing asymmetry: the first 2-intercept caustic being most responsive, the 3-intercept caustic slightly less so, and the third and second 2-intercept caustics even less so, in that order. Second, the angles between the opposing rays for each caustic appear to be fairly constant with changing asymmetry, except when one of the rays nears extinction by internal reflection.

Figures 8a, 8b, and 8c illustrate these points. Each of these figures is a plot of the propagation angle θ as a function of the percentage of γ

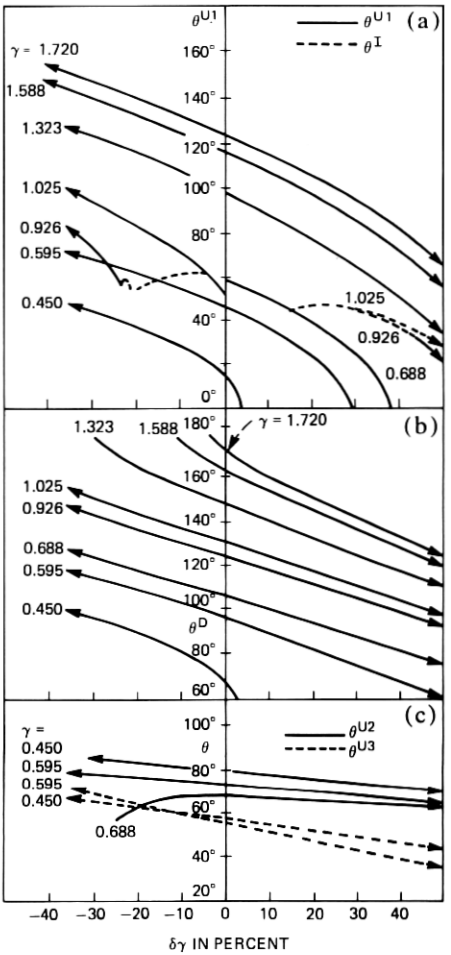

Fig. 8—Plots of the θ angles of the caustic trajectories for various γs as functions of the asymmetry, $\delta\gamma$. Here the values of the angles, θ_-, emergent on the side where γ is decreased are plotted on the left; the values of the angles, θ_+, emergent on the side where γ is increased are plotted on the right. These results are arranged as follows: (a) The first 2-intercept caustic angles, designated θ^{U1}, and the I ray propagation angle, θ^I, vs the asymmetry, $\delta\gamma$, in percent. (b) The 3-intercept caustic angle, θ^D, vs the asymmetry, $\delta\gamma$, in percent. (c) The second and third 2-intercept caustic angles, θ^{U2} and θ^{U3}, vs the asymmetry, $\delta\gamma$, in percent.

asymmetry, $\delta\gamma$. The values for the side where γ is decreased, θ_-, are plotted to the left; and the values for the side where γ is increased, θ_+, are plotted to the right of the zero asymmetry line. Figures 8a and 8b represent the response of the first 2-intercept and the 3-intercept caustics respectively, while the responses of both the second and third 2-intercept caustics are presented in Fig. 8c. The θ response of the I ray is represented by a broken curve where it appears alone on Fig. 8a, and broken curves are used in Fig. 8c to differentiate between the second and third

2-intercept caustics. Each curve shown is labeled to indicate the average γ for which the range of asymmetries is now determined. Thus, to determine the θ angles for a first 2-intercept caustic ray on a melt zone of average γ of 1.323 with an asymmetry of $\delta\gamma = \pm 30$ percent, one finds a value of 115 degrees on the left side of the plot as the value of θ_{-}^{U1} on the side of the melt zone where γ is reduced 30 percent, and a value of 77.4 degrees on the right of the plot as the value of θ_{+}^{U1} on the side of the melt zone where γ is increased 30 percent.

Except for those portions of the curves which are near points of extinction, the curves* for both the first 2-intercept caustic and the 3-intercept caustic are similar in shape for all γs. In fact, over the range of most realistic asymmetries, which means the first ± 10 or ± 15 percent, these curves are almost linear. This indicates that for these caustics the total included angle between opposing caustic rays, $\theta_{+} + \theta_{-}$, remains constant while the angle of its bisector increases linearly with the increasing asymmetry. In terms of actual drawdown samples, these caustic rays form cones of light which remain fairly stable in shape but which tilt in the direction of these asymmetries and become distorted in those regions where they approach extinction by internal reflection. This is also true of the second 2-intercept caustic except that it seems to be relatively less sensitive to this asymmetry.

Another way of illustrating this behavior is shown in Fig. 9. Here the average sum, $\theta_S = \frac{1}{2}(\theta_{-} + \theta_{+})$, is a direct measure of the constancy of the cone half-angle as a function of asymmetry, while the average difference, $\theta_D = \frac{1}{2}(\theta_{-} - \theta_{+})$, gives a direct measure of the tilt or rotation of the cone as a function of asymmetry. Figure 9a shows that the cone half-angle for the first 2-intercept caustic, θ_S^{U1}, remains fairly constant but does decrease a few degrees at high asymmetries. This may be partially accounted for by the fact that the average β angle does not remain constant with increasing asymmetry but decreases as shown in Fig. 10. Consequently, if the first 2-intercept caustic is somewhat more β-dependent, it too may be expected to decrease, since in Part I[1] on symmetric drawdowns it was shown that decreasing β decreases θ. On the other hand, Fig. 9b shows fairly constant 3-intercept caustic-ray cone angles, θ_S^D, for all circumstances except those approaching extinction, as does Fig. 9c for the θ_S angles of the second and third 2-intercept caustics.

In all plots of Fig. 9, the curves for the average differences, θ_D, vs

* Many more calculations were made to produce these plots than were illustrated by the diagrams of Fig. 7, with particular attention given to accurate determination of the points where each caustic disappeared, if it did so within the range of interest. These terminations are shown exactly where they occur on the plots of Fig. 8, with arrows marking a continuation where the computation was stopped for other reasons, such as reaching the limits of the maximum range of interest or reaching the limits of the computable range of the input data.

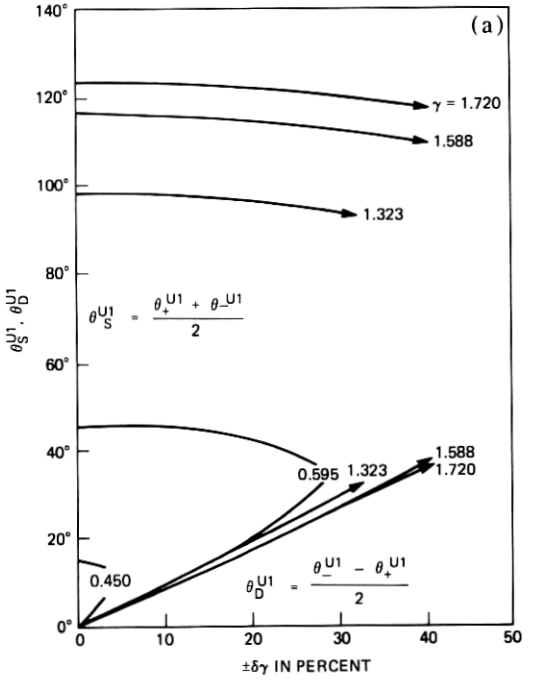

Fig. 9—Plots of the averaged sums, $\theta_S = \frac{1}{2}(\theta_- + \theta_+)$, and the averaged differences, $\theta_D = \frac{1}{2}(\theta_- - \theta_+)$, vs the asymmetry, $\delta\gamma$, for various γs. These results are arranged as shown in 9a, 9b, and 9c. (a) The first 2-intercept caustic angle's averaged sums and differences vs the asymmetry, $\pm\delta\gamma$, in percent. (*Figs. 9b and 9c on following pages.*)

asymmetry, $\delta\gamma$, are nearly linear within the same limitation and indicate a constant slope or rate of rotation, r_D. The greater slopes, r_D, of the average difference curves in Fig. 9a indicate the higher response of the first 2-intercept caustic to changes in asymmetry, which is about 0.8 degree/±1 percent. Also, their closer grouping indicates a significant degree of uniformity of this rate over a range of γs. The θ_D vs $\delta\gamma$ curves for the 3-intercept caustic ray angles are also nearly linear but shallower, with rates of rotation, r_D, of about 0.6 degree/±1 percent. They also show considerably more variation from γ to γ.

Figure 9c shows the same two functions (θ_S vs $\delta\gamma$ and θ_D vs $\delta\gamma$) for the second and third 2-intercept caustics. For both, the half-cone angles, θ_S, are reasonably constant except near extinction (i.e., the second caustic at $\gamma = 0.68$ degree), but the rates of rotation are smaller. These run from 0.4 degree/±1 percent and less for the third caustic to 0.17 degree/±1 percent and slightly negative for the second caustic, and with much greater variation from γ to γ.

The results provide a means by which the caustic angles measured on opposite sides of a section through the melt zone may be used to estimate both average γ and its asymmetry for that section. For example, since

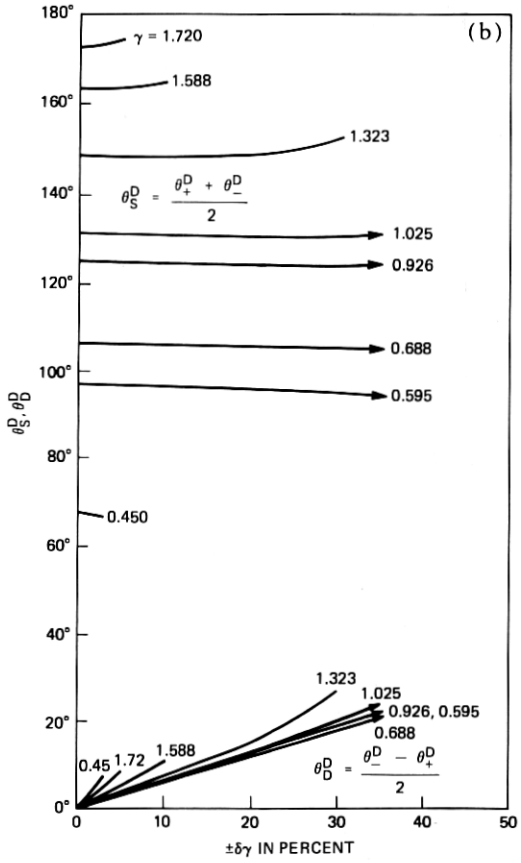

Fig. 9(b)—The 3-intercept caustic angle's averaged sums and differences vs the asymmetry, ± $\delta\gamma$, in percent.

the averaged sum of the 3-intercept caustic angles, θ_S^D, is relatively insensitive to the asymmetry in γ (Fig. 9b), this parameter may be used to estimate γ. In other words, θ_S^D will be very nearly the same as θ^D for the symmetric case. In turn, the dependence on γ may be derived directly from the θ^D vs β relationship given in Fig. 6 of Part I.[1] Figure 11 shows a plot of θ_S^D vs γ adapted from this original plot of θ^D vs β using $\gamma = \tan \beta$ and $\theta_S^D \approx \theta^D$. The figure also shows a plot of the inverse rate of rotation, r_D^{-1} vs γ. Therefore, for a drawdown where melt zone asymmetry is the result of an asymmetry in γ, measurement of θ_+^D and θ_-^D will provide a means of estimating γ and its asymmetry as follows:

From θ_-^D and θ_+^D, compute $\theta_D^D = \frac{1}{2}(\theta_-^D - \theta_+^D)$ and $\theta_S^D = \frac{1}{2}(\theta_-^D + \theta_+^D)$. Then use Fig. 11 to estimate a value of γ and to find the corresponding value of r_D^{-1}. The latter may then be used to compute the asymmetry, $\delta\gamma$, by multiplying by θ_D^D. Consider the example of a sample whose 3-intercept caustic angles measure 134 and 115 degrees. These yield a

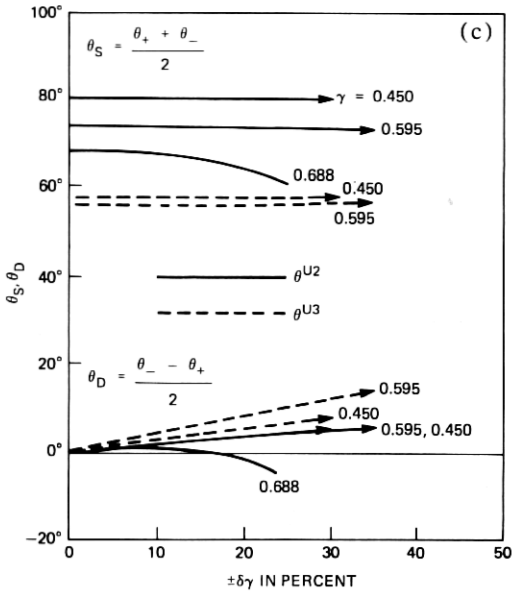

Fig. 9(c)—The second and third 2-intercept caustic angles' averaged sums and differences vs the asymmetry, ± $\delta\gamma$, in percent.

θ_S^D = 124.5 degrees which, by Fig. 11, gives an estimated γ of 0.930. At this γ, Fig. 11 also gives an r_D^{-1} = 1.56. Since θ_D^D = 9.5 degrees, the asymmetry, $\delta\gamma$, is then 1.56 ×.9.5 = 14.8 percent. Computer-generated data for a γ of 0.926 with an asymmetry of ±15 percent gives θ_-^D = 134.1 degrees and θ_+^D = 115.0 degrees, which is within an absolute error of only 0.004 in estimating γ and 0.2 percent in estimating the asymmetry. This order of accuracy is consistent throughout the region for which θ_S^D is independent of γ.

The development of additional data for the various 2-intercept caustics would permit similar analyses of data taken over the appropriate γ or β ranges for which these caustics appear on both sides of the melt zone and manifest linear dependences on $\delta\gamma$ or $\delta\beta$.

IV. COMPARISON WITH AN ACTUAL DRAWDOWN SAMPLE

Empirical profile data from Sample 1 discussed in Ref. 2 provide a comparison for the present technique. Figure 12 shows data taken from the 3 and 9 o'clock profiles superimposed on smooth curves computed from the averaged data used in the present report (from Sample 4). These synthesized profiles have been asymmetrically scaled (γ = 1.006 ± 15 percent) to match the β angles of the empirical data (β_+ = 48.9 degrees (3-side) and β_- = 44.6 degrees (9-side)). It can be seen that the empirical and computed values are very similar and superimposed (in this case) with no axial shift asymmetry ($\Delta/\gamma R$ = 0). Various caustic

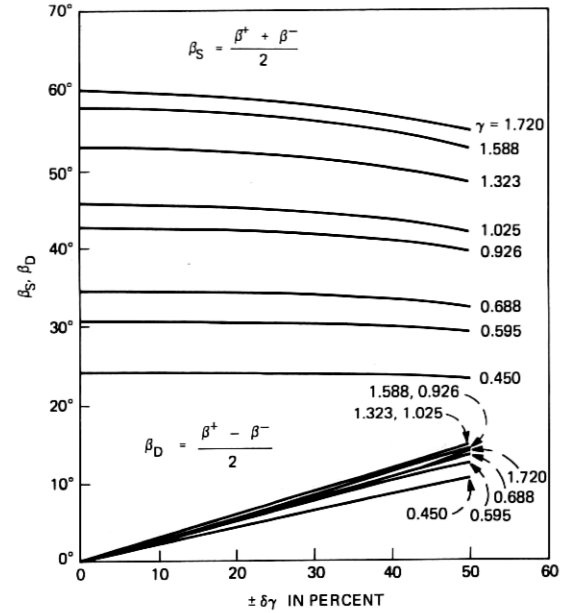

Fig. 10—Plots of the averaged sums, $\beta_S = \frac{1}{2}(\beta_- + \beta_+)$, and the averaged differences, $\beta_D = \frac{1}{2}(\beta_- - \beta_+)$, vs the asymmetry, $\delta\gamma$, in percent, for various γs. Here β_- is the incident angle on the side of reduced γ and β_+ is the incident angle on the side of increased γ.

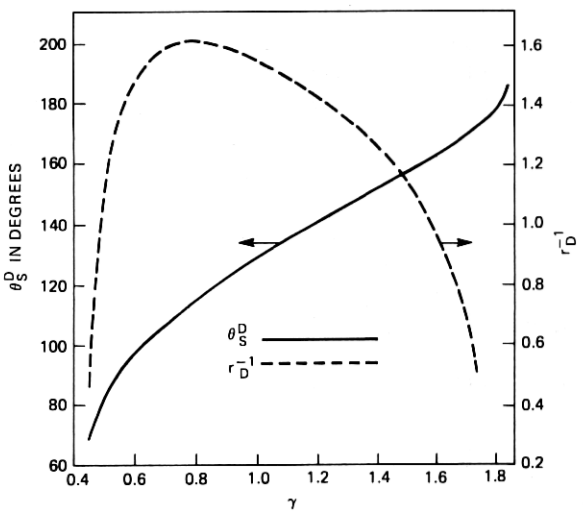

Fig. 11—Plots of the averaged sum of the caustic angles, θ_S^D, and the inverse rate of rotation (from their averaged difference curves), r_D^{-1}, vs γ for the 3-intercept caustics.

angles were computed from these profiles and are shown in Table II along with the angles measured in the original experiment and the values calculated at that time using the empirical profile data. In some cases,

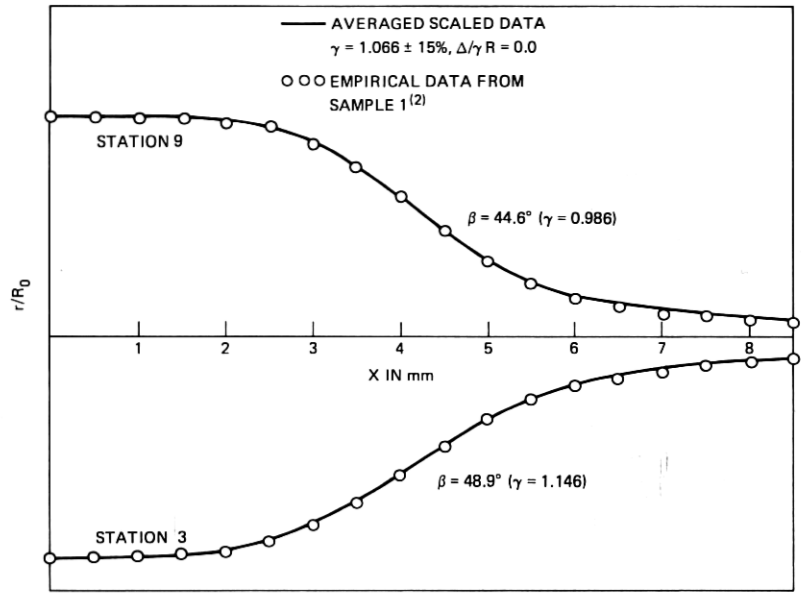

Fig. 12—Plots of the empirical profile data from Sample 1 (Ref. 2) and the computed profiles obtained using the present technique for synthesizing asymmetric profiles (γ = 1.006 ± 15 percent, $\Delta/\gamma R = 0$) with differing slopes ($\beta_+ = 48.9$ degrees, $\beta_- = 44.6$ degrees). For Sample 1, $R_0 = 3.24$ mm, and for Sample 4, $R_0 = 3.09$ mm.

Table II—Caustic angles from profile data

	Measured Values From Original Experiments (Ref. 2) (degrees)	Calculated Values Using Empirical Profile Data (Sample 1) (degrees)	Computed Values Using Smoothed Avg'd Data (Sample 4) (degrees)
θ_+^U	46.1	54.5	EXT (43.2)*
θ_-^U	72.5	75.3	75.0
θ_+^D	130.6	133.8	122.1
θ_-^D	140.0	142.7	145.4
θ_S^U	59.3	64.9	(59.1)*
θ_S^D	135.3	138.3	133.8
θ_D^U	13.2	10.4	(15.9)*
θ_D^D	4.7	4.5	11.7

* In this case the caustic is extinguished by internal reflection, so the extinction angle itself is used in computing effective θ_S^U and θ_D^U values.

the newer values are in better agreement with the observed angles than are those computed using the actual profiles, and certainly they appear to be about as good overall.

V. SUMMARY

Two types of asymmetry have been studied using computer simulation for predicting the trajectories of caustics emitted by a coaxially illuminated, fused-silica melt zone. The first type of asymmetry involves an

axial shift of one side of the melt zone with respect to the other. Increases in this type of asymmetry produce changes in the trajectories of the various types of caustics which appear. The appearance of these caustics also depends very strongly upon the average taper of the melt zone.[2] The following effects have been observed:

(*i*) The first 2- and 3-intercept caustics rotate downstream when they appear on the trailing side of the melt zone.

(*ii*) The first 2-intercept caustic initially starts to rotate upstream and then reverses direction when it appears on the leading side. This effect is more pronounced in blunter melt zones.

(*iii*) The first 3-intercept caustic generally rotates upstream on the leading side but may reverse its rotation for large asymmetries on very blunt melt zones.

(*iv*) The second 3-intercept caustic appears on the leading side only for blunt melt zones ($\gamma = 0.450$) and only at large asymmetries for which it rotates downstream.

(*v*) The second and third 2-intercept caustics rotate downstream on the leading side and upstream on the trailing side with increasing asymmetry. This is the reverse rotation of the first two major caustics.

(*vi*) The fourth 2-intercept caustic appears only on the leading side of melt zones which are moderately blunt ($\gamma \leq 0.688$) and rotates downstream with increasing asymmetry.

(*vii*) When a particular caustic appears on opposite sides of a melt zone, its intersecting trajectories form an angle which may be thought of as the included angle of a cone of light emitted from a three-dimensional sample.* Cone angles of the first 3-intercept caustic and the second and third 2-intercept caustics are moderately insensitive to the asymmetry.

(*viii*) The cone angle of the first 2-intercept caustic increases significantly with increasing asymmetry.

(*ix*) The cones of light for most of these caustics rotate forward with increasing asymmetry. The rotation of the cones of light for the 3-intercept caustic and the first 2-intercept caustic is initially forward or toward the leading side and then reverses.

(*x*) The light cones for the second and third 2-intercept caustics generally rotate backward at a constant rate with increasing asymmetry for a given γ.

(*xi*) The rate of rotation of the first 3-intercept caustic is generally greater than that of the first 2-intercept caustic, while the rates of rotation for the second and third 2-intercept caustics are always negative.

* It should be kept in mind that the cone angle, as we have defined it here, is the sum of the particular caustic angles on opposite sides of the drawdown measured from the upstream axial direction.

The second type of asymmetry investigated involves scaling opposite sides of the melt zone differently to produce asymmetries in slope. Increases in slope asymmetry produce changes in the external caustic trajectories, which are in many ways simpler than those observed with the axial shift asymmetry. These changes are as follows.

(*i*) All caustics generally rotate downstream on the trailing (decreased) γ side and upstream on the leading (increased) γ side. This is comparable to the behavior of the first 2- and 3-intercept caustic response to the shift asymmetry.

(*ii*) The cone angles of the 3-intercept caustic and the second and third 2-intercept caustics are almost independent of the asymmetry over significant ranges.

(*iii*) The cone angle of the first 2-intercept caustic is only weakly dependent on the asymmetry in γ and may be varying in response to changes in the average value of β, which itself changes with asymmetry.

(*iv*) There is no second 3-intercept caustic, as was the case previously.

(*v*) All the caustics rotate forward at constant rates for any particular γ.

(*vi*) The rates of rotation are ordered as follows:

$$r_{U1} > r_D > r_{U3} > r_{U2}.$$

For both types of asymmetry, sufficient rotation in any axial plane usually causes one of the caustic trajectories to be extinguished by internal reflection. The approach of a caustic trajectory to its extinction usually results in an acceleration in its rate of rotation, thereby distorting the general pattern of movement of the cone of light for that caustic. Nevertheless, over much of the range of reasonable geometries there will be caustics whose rotations are sufficiently regular as to provide a direct means of estimating the geometrical asymmetry from the asymmetry of the caustic cone itself, if the caustic and type of asymmetry are properly identified.

VI. ACKNOWLEDGMENT

The authors wish to acknowledge the collaboration of J. McKenna, who contributed to the development of the numerical algorithm.

REFERENCES

1. T. D. Dudderar, J. B. Seery, and P. G. Simpkins, "Caustic Patterns Associated With Melt Zones in Solidified Glass Samples—Part I: Symmetric Cases," B.S.T.J., this issue, pp. 3209–3225.
2. P. G. Simpkins, T. D. Dudderar, J. McKenna, and J. B. Seery; "On the Occurrence of Caustics in the Drawdown Zone of Silica Fibers," B.S.T.J., *56*, No. 4 (April 1977), pp. 535–560.